Radiology

ORIGINAL RESEARCH • PEDIATRIC IMAGING

MRI Features for Identifying *MYCN*-amplified *RB1* Wild-type Retinoblastoma

Robin W. Jansen, MD • Christiaan M. de Bloeme, MD • Liesbeth Cardoen, MD • Sophia Göricke, MD • Sabien van Elst, MSc • Jaime Lyn Jessen, MSc, CGC, CCGC • Aparna Ramasubramanian, MD • Alison H. Skalet, MD, PhD • Audra K. Miller, MD • Philippe Maeder, MD • Ogul E. Uner, MD • G. Baker Hubbard, MD • Hans Grossniklaus, MD, MBA • H. Culver Boldt, MD • Kim E. Nichols, MD • Rachel C. Brennan, MD • Saugata Sen, MD • Selma Sirin, MD, PhD • Hervé J. Brisse, MD, PhD • Paolo Galluzzi, MD • Charlotte J. Dommering, MD, PhD • Jonas A. Castelijns, MD, PhD • Paul van der Valk, MD, PhD • Ronald Boellaard, MSc, PhD • Josephine Dorsman, MSc, PhD • Annette C. Moll, MD, PhD • Marcus C. de Jong, MD, PhD • Pim de Graaf, MD, PhD

From the Departments of Radiology and Nuclear Medicine (R.W.J., C.M.d.B., S.v.E., J.A.C., R.B., M.C.d.J., P.d.G.), Human Genetics (C.J.D.), Pathology (P.v.d.V.), Oncogenetics (J.D.), and Ophthalmology (A.C.M.), Amsterdam University Medical Center, Vrije Universiteit, Office PK-1X012, De Boelelaan 1117, 1081 HV Amsterdam, the Netherlands; Cancer Center Amsterdam, Amsterdam, the Netherlands (R.W.J., C.M.d.B., S.v.E., J.D., A.C.M., M.C.d.J., P.d.G.); European Retinoblastoma Imaging Collaboration (R.W.J., C.M.d.B., L.C., S.G., P.M., H.C.B., P.G., J.A.C., M.C.d.J., P.d.G.); Imaging Department, Institut Curie Paris, Paris, France (L.C., H.J.B.); Institute of Diagnostic and Interventional Radiology and Neuroradiology, University Hospital Essen, Essen, Germany (S.G.); Impact Genetics–Dynacare, Brampton, Canada (J.L.J.); Department of Ophthalmology, Phoenix Children's Hospital, Phoenix, Ariz (A.R.); Casey Eye Institute & Knight Cancer Institute, Oregon Health & Science University, Portland, Ore (A.H.S., A.K.M.); Department of Radiology, Centre Hospitalier Universitaire Vaudois, Lausanne, Switzerland (P.M.); Department of Ophthalmology, Casey Eye Institute, Oregon Health & Science University, Portland, Ore (O.E.U.); Ocular Oncology Service, Emory Eye Center, Atlanta, Ga (O.E.U., G.B.H., H.G.); Department of Ophthalmology, University of Iowa Hospitals & Clinics, Iowa City, Iowa (H.C.B.); Department of Oncology, St Jude Children's Research Hospital, Memphis, Tenn (K.E.N., R.C.B.); Department of Pediatric Hematology/Oncology, Logan Health, Kalispell, Mont (R.C.B.); Department of Radiology and Imaging Sciences, Tata Medical Center, Kolkata, India (S. Sen); Department of Diagnostic Imaging, University Children's Hospital Zürich, Zürich, Switzerland (S. Sirin); and Azienda Ospedaliera Universitaria Senese, Siena, Italy (P.G.). Received September 16, 2022; revision requested November 18; revision received March 6, 2023; accepted March 20. **Address correspondence to** R.W.J. (email: *r.jansen1@amsterdamumc.nl*).

Initiation and coordination of this study was funded by Stichting Kinderen Kankervrij (KIKA) (grant no. 342) and the Hanarth Foundation (grant for project titled *MRI-based Deep Learning Segmentation and Quantitative Radiomics in Retinoblastoma: A Next Step Toward Personalized Interventions*). Departmental funding was received by Casey Eye Institute, Oregon Health & Science University (A.H.S., A.K.M., and O.E.U.) from the National Institutes of Health (grant P30 EY010572) in addition to unrestricted departmental funding from Research to Prevent Blindness. Departmental funding was received by Emory Eye Center, Ocular Oncology Service (O.E.U., G.B.H., and H.G.) via National Eye Institute core grant P30 EY006360.

Conflicts of interest are listed at the end of this article.

See also the editorial by Rollins in this issue.

Radiology 2023; 307(5):e222264 • https://doi.org/10.1148/radiol.222264 • Content codes: HN MR

Background: *MYCN*-amplified *RB1* wild-type ($MYCN^{A}RB1^{+/+}$) retinoblastoma is a rare but clinically important subtype of retinoblastoma due to its aggressive character and relative resistance to typical therapeutic approaches. Because biopsy is not indicated in retinoblastoma, specific MRI features might be valuable to identify children with this genetic subtype.

Purpose: To define the MRI phenotype of $MYCN^{A}RB1^{+/+}$ retinoblastoma and evaluate the ability of qualitative MRI features to help identify this specific genetic subtype.

Materials and Methods: In this retrospective, multicenter, case-control study, MRI scans in children with $MYCN^{A}RB1^{+/+}$ retinoblastoma and age-matched children with $RB1^{-/-}$ subtype retinoblastoma were included (case-control ratio, 1:4; scans acquired from June 2001 to February 2021; scans collected from May 2018 to October 2021). Patients with histopathologically confirmed unilateral retinoblastoma, genetic testing (*RB1/MYCN* status), and MRI scans were included. Associations between radiologist-scored imaging features and diagnosis were assessed with the Fisher exact test or Fisher-Freeman-Halton test, and Bonferroni-corrected *P* values were calculated.

Results: A total of 110 patients from 10 retinoblastoma referral centers were included: 22 children with $MYCN^{A}RB1^{+/+}$ retinoblastoma and 88 control children with $RB1^{-/-}$ retinoblastoma. Children in the $MYCN^{A}RB1^{+/+}$ group had a median age of 7.0 months (IQR, 5.0–9.0 months) (13 boys), while children in the $RB1^{-/-}$ group had a median age of 9.0 months (IQR, 4.6–13.4 months) (46 boys). $MYCN^{A}RB1^{+/+}$ retinoblastomas were typically peripherally located (in 10 of 17 children; specificity, 97%; $P < .001$) and exhibited plaque or pleomorphic shape (in 20 of 22 children; specificity, 51%; $P = .011$) with irregular margins (in 16 of 22 children; specificity, 70%; $P = .008$) and extensive retina folding with vitreous enclosure (specificity, 94%; $P < .001$). $MYCN^{A}RB1^{+/+}$ retinoblastomas showed peritumoral hemorrhage (in 17 of 21 children; specificity, 88%; $P < .001$), subretinal hemorrhage with a fluid-fluid level (in eight of 22 children; specificity, 95%; $P = .005$), and strong anterior chamber enhancement (in 13 of 21 children; specificity, 80%; $P = .008$).

Conclusion: $MYCN^{A}RB1^{+/+}$ retinoblastomas show distinct MRI features that could enable early identification of these tumors. This may improve patient selection for tailored treatment in the future.

Supplemental material is available for this article.

Retinoblastoma is the most common malignant eye tumor in children (incidence of one in 17 000 live births), usually diagnosed before the child reaches 5 years of age (1). Tumorigenesis is predominantly initiated by two genetic events involving both alleles of the tumor suppressor gene *RB1* (ie, $RB1^{-/-}$ retinoblastoma). A new molecular subtype of retinoblastoma without pathogenic variants in the *RB1* gene ($RB1^{+/+}$) has been

Abbreviation

MYCN^{A}*RB1*$^{+/+}$ = *MYCN*-amplified *RB1* wild-type

Summary

MYCN-amplified *RB1* wild-type retinoblastoma has distinct features compared with *RB1* pathogenic variant–driven retinoblastoma at MRI, including tumors in a peripheral (anterior) location with plaque or pleomorphic shape, irregular margins, tumor-retinal folding, and peritumoral blood.

Key Results

- In this retrospective study of 110 patients, unique MRI features enabled differentiation of patients with *MYCN*-amplified *RB1* wild-type retinoblastoma (*MYCN*^{A}*RB1*$^{+/+}$) (n = 22) from patients with *RB1* pathogenic variant–driven retinoblastoma (n = 88).
- MRI features that showed high specificity for *MYCN*^{A}*RB1*$^{+/+}$ identification included peripheral location (anteriorly to the equator) (97%; P < .001), peritumoral hemorrhage (88%; P < .001), subretinal hemorrhage with a fluid-fluid level (95%; P = .005), and tumor-retinal folding with vitreous enclosure (94%; P < .001).

discovered. Instead, a high level of *MYCN* amplification was found to be the driving force in the initiation of retinal tumors (*MYCN*-driven or *MYCN*-amplified *RB1* wild-type [*MYCN*^{A}*RB1*$^{+/+}$] retinoblastoma) in approximately 1%–2% of patients with retinoblastoma (2–5). Although *MYCN* amplifications also exist in *RB1*$^{-/-}$ tumors, the clinical appearance suggests a distinct phenotype for *RB1*$^{+/+}$ tumors driven by *MYCN* amplification (6,7). This *MYCN*^{A}*RB1*$^{+/+}$ subtype was found to be a unilateral subtype and manifests with larger tumors in children at a very young age; it showed strikingly distinct histopathologic features with poorly differentiated tumors consisting of neuroblastic cells and few rosettes (2). Additionally, a relative resistance to typical therapeutic approaches was found (8). While eye-preserving treatment is increasingly attempted in the children with *MYCN*^{A}*RB1*$^{+/+}$ retinoblastoma, salvaging an eye in this aggressive subtype of retinoblastoma may result in a higher risk of uncontrolled disease. Therefore, early identification of patients with *MYCN*^{A}*RB1*$^{+/+}$ retinoblastoma is clinically important and may enable a distinct treatment approach.

Detecting genetic traits of retinoblastoma is increasingly challenging in clinical practice due to the lack of availability of histopathologic material for molecular testing. Tumor biopsy is contraindicated because of the associated risk of local tumor seeding and metastasis. Furthermore, enucleated specimens have become less available due to the increasing use of eye-saving treatment options, even in advanced stages (9,10). Development of noninvasive stratification methods is therefore important for subtype recognition and implementation of novel targeted therapies. The recently emerging minimally invasive technique of obtaining cell-free tumor DNA from the aqueous humor may become advantageous (11). MRI similarly has great potential for molecular subtype differentiation with the advantages of being noninvasive and widely used in children with retinoblastoma for supporting the diagnosis, examining disease extent, and screening for intracranial disease (12–15). The imaging phenotype of *MYCN*^{A}*RB1*$^{+/+}$ retinoblastoma, however, remains unclear. The purpose of this study was to assess MRI features of *MYCN*^{A}*RB1*$^{+/+}$ retinoblastoma and to evaluate whether this genetic subtype can be differentiated from *RB1*$^{-/-}$ retinoblastoma using qualitative MRI features.

Materials and Methods

Patients

The institutional review board of Vrije Universiteit University Medical Center (institutional review board no. 00002991) in Amsterdam, the Netherlands, approved this multicenter, retrospective, case-control study; the requirement to obtain informed consent was waived. This study was performed in accordance with the Standards for Reporting of Diagnostic Accuracy Studies, or STARD, statement guidelines.

MRI scans from patients with retinoblastoma were retrospectively collected. MRI scans were acquired between June 2001 and February 2021 and collected between May 2018 and October 2021 from retinoblastoma referral centers. Case identification was performed by addressing both published authors who studied patients with *MYCN*^{A}*RB1*$^{+/+}$ retinoblastoma and retinoblastoma referral centers. Six patients (three from Germany and three from the Netherlands) were previously reported in the first report, to our knowledge, on the *MYCN*^{A}*RB1*$^{+/+}$ subtype retinoblastoma (2) and one patient (from India) was previously reported in a case report (8). For each identified patient with the *MYCN*^{A}*RB1*$^{+/+}$ retinoblastoma subtype, matched controls with *RB1*$^{-/-}$ retinoblastoma were included at a ratio of 1:4. Inclusion criteria were *(a)* histopathologically confirmed diagnosis of retinoblastoma, *(b)* unilateral disease, *(c)* MRI examination performed after 1995 and including at least noncontrast T1-weighted and gadolinium-based contrast agent–enhanced T1-weighted sequences, and *(d)* genetic analysis of tumor material: for *MYCN*^{A}*RB1*$^{+/+}$ retinoblastomas, this included *MYCN* amplification and *RB1* wild-type expression, and for *RB1*$^{-/-}$ retinoblastomas, this included biallelic *RB1* pathogenic variants. Genetic information was collected retrospectively; no genetic tests were performed for the current study. Case-control matching was performed based on age, date of MRI examination, and referral site. In instances where control MRI examinations from the same institution were unavailable, control MRI examinations from a different institution were used.

MRI Feature Selection and Assessment

MRI features were adopted from a previously validated imaging atlas of retinoblastoma (Table S1) (16). These included tumor morphologic features (location, growth pattern, shape) and tumor composition (homogeneity, calcifications, enhancement, necrosis). Three imaging features were added: *(a)* peritumoral hemorrhage (focal hypointense signal intensity on T2-weighted images specifically covering the surface of the tumor); *(b)* tumor-retinal folds with vitreous enclosure; and *(c)* a detached hyaloid membrane. The three added features were defined after unblinded review by independent readers not involved in further feature scoring (C.M.d.B. and R.W.J., with 4 and 5 years of experience, respectively, in ocular MRI). Subsequently, two radiologists with expertise in retinoblastoma imaging (P.d.G. and

M.C.d.J., with 10 and 17 years of experience, respectively, in ocular MRI) blinded to patient details (including age and genetic information) individually assessed all MRI scans for all features. Disagreements were resolved by consensus in a separate meeting. Imaging features that were marked as indeterminate after consensus were excluded from analysis (eg, the feature "subretinal seeding" is indeterminate in cases without retinal detachment). No central pathology review was performed, but histopathologic examinations were reviewed in six patients from the Netherlands to be able to demonstrate radiopathologic correlations.

Statistical Analysis

Interobserver MRI reader variability was assessed by calculating Fleiss κ. Data distribution was assessed using the Shapiro-Wilk test. The two-tailed Fisher exact test and Fisher-Freeman-Halton test were used for the statistical analyses. Bonferroni-corrected $P < .05$ was considered indicative of statistically significant difference. Statistical calculations were performed using SPSS software (version 26, IBM).

Results

Patients

Of the 110 patients with retinoblastoma included in the study, 22 had the *MYCN*^{A}*RB1*$^{+/+}$ molecular subtype and 88 had the *RB1*$^{-/-}$ molecular subtype. Data for patients with *MYCN*^{A}*RB1*$^{+/+}$ retinoblastoma were included from 10 retinoblastoma referral centers in Amsterdam, the Netherlands ($n = 6$); Paris, France ($n = 4$); Essen, Germany ($n = 3$); Phoenix, Arizona, U.S. ($n = 2$); Portland, Oregon, U.S. ($n = 2$); Lausanne, Switzerland ($n = 1$); Atlanta, Georgia, U.S. ($n = 1$); Iowa City, Iowa, U.S. ($n = 1$); Memphis, Tennessee, U.S. ($n = 1$); and Kolkata, India ($n = 1$). Figure 1 demonstrates the identification and inclusion process for patients in this study. No patients were excluded. Patient demographic characteristics are available in Table 1; the case-control study design resulted in similar groups with no significant differences in patient age or the year of the MRI examination.

Tumor Characteristics of *MYCN*^{A}*RB1*$^{+/+}$ Retinoblastoma

Identified associations between imaging features and the *MYCN*^{A}*RB1*$^{+/+}$ subtype of retinoblastoma are listed in Table 2; features scored as indeterminate resulted in patient numbers not always adding up to the total of 22 patients with *MYCN*^{A}*RB1*$^{+/+}$ retinoblastoma and 88 patients with *RB1*$^{-/-}$ retinoblastoma. A peripheral tumor location (anteriorly to the equator) showed a 97% specificity for *MYCN*^{A}*RB1*$^{+/+}$ retinoblastoma and was found in 59% of children with *MYCN*^{A}*RB1*$^{+/+}$ retinoblastoma (10 of 17) compared with 2.6% of children with *RB1*$^{-/-}$ retinoblastoma (two of 77) ($P < .001$) (Fig 1). Extensive retinal folds were found in the *MYCN*^{A}*RB1*$^{+/+}$ subtype, in which the tumor-affected retina was seen to enclose parts of the vitreous (Figs 1–3). This MRI feature showed a specificity of 94% for the *MYCN*^{A}*RB1*$^{+/+}$ subtype and was present in 58% of children with *MYCN*^{A}*RB1*$^{+/+}$ retinoblastoma (11 of 19) versus in 5.9% of children with *RB1*$^{-/-}$ (five of 85) ($P < .001$). Another MRI feature associated with the *MYCN*^{A}*RB1*$^{+/+}$ subtype was irregular tumor margins, which occurred in 73% of patients with *MYCN*^{A}*RB1*$^{+/+}$ (16 of 22) versus 30% of patients with *RB1*$^{-/-}$ retinoblastoma (26 of 86) (specificity, 70%; $P = .008$) (Fig 3). *MYCN*^{A}*RB1*$^{+/+}$ retinoblastomas more frequently had plaque or pleomorphic shape (in 20 of 22 children [91%]) compared with *RB1*$^{-/-}$ retinoblastomas (in 43 of 87 children [49%]), with the latter showing relatively more dome- or lens-shaped tumors ($P = .011$) (Fig 3). Additionally, a larger number of tumor foci ($P = .005$) and a diffuse infiltrative growth pattern ($P = .044$) were found to be associated with *MYCN*^{A}*RB1*$^{+/+}$ retinoblastoma. Table S1 lists the frequency and interobserver agreement of all assessed imaging features. The frequency of individual imaging features showed a wide range (0%–91%), as did the interobserver agreement (κ = 0.03–0.81).

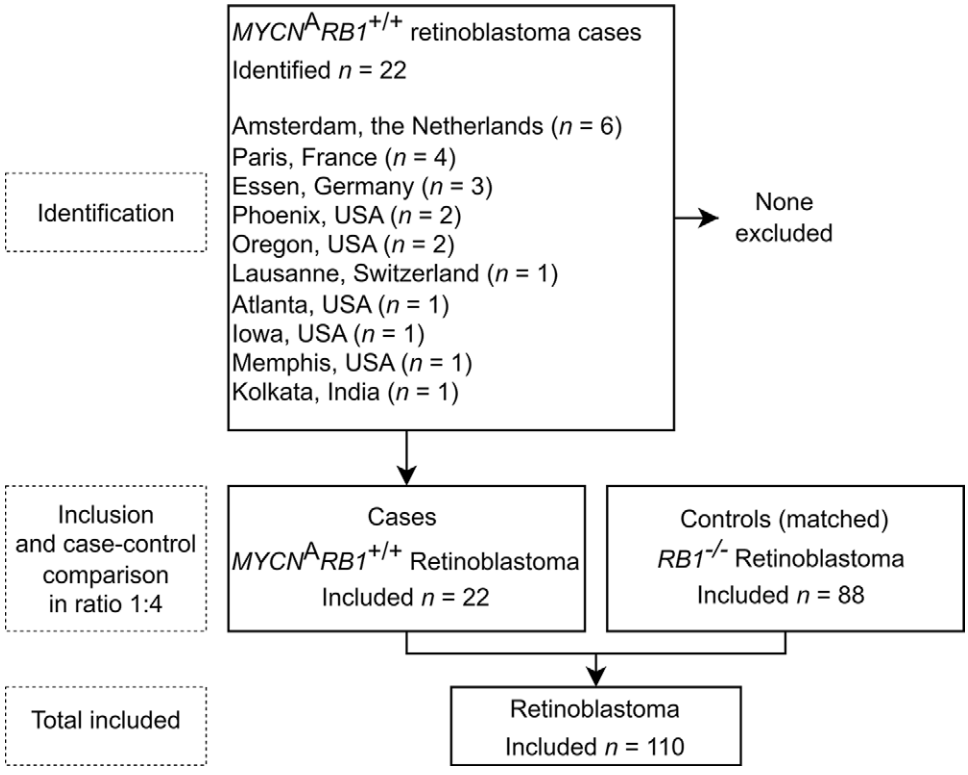

Figure 1: Flowchart diagram shows inclusion of patients in this case-control study with a ratio between cases and controls of 1:4. Cases are patients with *MYCN*-amplified *RB1* wild-type (*MYCN*^{A}*RB1*$^{+/+}$) retinoblastoma, and controls are patients with biallelic pathogenic variation of *RB1*–driven (ie, *RB1*$^{-/-}$) retinoblastoma.

Table 1: Patient Demographic Characteristics

Characteristic	Patients with $MYCN^{A}RB1^{+/+}$ Retinoblastoma (n = 22)	Patients with $RB1^{-/-}$ Retinoblastoma (n = 88)	Total Patients (n = 110)	P Value
Sex				.64
F	9 (41)	42 (48)	51 (46)	
M	13 (59)	46 (52)	59 (54)	
Laterality (left eye)	10 (46)	46 (52)	56 (51)	.64
Age at MRI examination (mo)*	7.0 (5.0–9.0)	9.0 (4.6–13.4)	8.0 (3.5–12.5)	.14
Mode for MRI examination year	2018	2017	2017	
Range for MRI examination year	2002–2021	2001–2021	2001–2021	

Note.—Unless otherwise specified, data are numbers of patients, with percentages in parentheses. P values were derived using the Fisher exact test or independent sample t test. $MYCN^{A}RB1^{+/+}$ = *MYCN*-amplified *RB1* wild-type, $RB1^{-/-}$ = *RB1* pathogenic variants.

* Data are medians, with IQRs in parentheses.

Table 2: Radiologist-assessed MRI Features of $MYCN^{A}RB1^{+/+}$ Retinoblastoma Compared with $RB1^{-/-}$ Retinoblastoma

MRI Feature	Feature Outcome	Patients with $MYCN^{A}RB1^{+/+}$ Retinoblastoma	Patients with $RB1^{-/-}$ Retinoblastoma	P Value	Sensitivity (%)	Specificity (%)
Peripheral or anterior tumor location (greater part in front of equator vs behind equator)	Present	59 (10/17)	2.6 (2/77)	<.001*	59 [33, 82]	97 [91, 100]
Irregular tumor margins	Present	73 (16/22)	30 (26/86)	.008*	73 [50, 89]	70 [60, 80]
Plaque or pleomorphic shape (vs dome or lens shape)	Present	91 (20/22)	49 (43/87)	.011*	91 [71, 99]	51 [40, 61]
Peritumoral hemorrhage	Present	81 (17/21)	12 (10/83)	<.001*	81 [58, 95]	88 [79, 94]
Subretinal hemorrhage with fluid-fluid level	Present	36 (8/22)	4.5 (4/88)	.005*	36 [17, 59]	95 [89, 99]
Strong enhancement of the anterior eye segment	Present	62 (13/21)	20 (17/84)	.008*	62 [38, 82]	80 [70, 88]
Tumor-retinal folds with enclosure of vitreous	Present	58 (11/19)	5.9 (5/85)	<.001*	58 [34, 80]	94 [87, 98]
No. of lesions				.005†		
	1 lesion	19 (4/21)	65 (57/88)			
	1–5 lesions	24 (5/21)	15 (13/88)			
	6–10 lesions	10 (2/21)	3.4 (3/88)			
	>10 lesions	48 (10/21)	17 (15/88)			
Growth pattern				.044†		
	Diffuse growth	23 (5/22)	2.4 (2/85)			
	Endophytic growth	4.5 (1/22)	22 (19/85)			
	Exophytic growth	73 (16/22)	75 (64/85)			

Note.—Unless otherwise specified, data are percentages, with numbers of patients in parentheses and 95% CIs in brackets. Features scored as indeterminate were not included in analysis; thus, numbers of patients do not always add up to 22 for *MYCN*-amplified *RB1* wild-type ($MYCN^{A}RB1^{+/+}$) retinoblastoma or 88 for $RB1^{-/-}$ retinoblastoma (ie, retinoblastoma with *RB1* pathogenic variants). Bonferroni-corrected P values are presented.

* P values calculated using the Fisher exact test.

† P values calculated using the Fisher-Freeman-Halton test.

Peritumoral Intraocular Findings in $MYCN^{A}RB1^{+/+}$ Retinoblastoma

Peritumoral hemorrhage was more often observed at MRI of $MYCN^{A}RB1^{+/+}$ retinoblastoma (in 17 of 21 children [81%]) compared with MRI of $RB1^{-/-}$ retinoblastoma (in 10 of 83 children [12%]) and was also apparent at histopathologic examination in a patient with both MRI and histopathologic data available (Fig 4). Additionally, children with $MYCN^{A}RB1^{+/+}$ retinoblastoma showed more subretinal blood to the extent that there was a fluid-fluid level present ($MYCN^{A}RB1^{+/+}$, eight of 22 children [36%]; $RB1^{-/-}$, four of 88 children [4.5%]), a finding that showed 95% specificity for *MYCN*-amplified tumors. Moreover, the *MYCN*-amplified tumors showed a more intense enhancement within the anterior eye segment

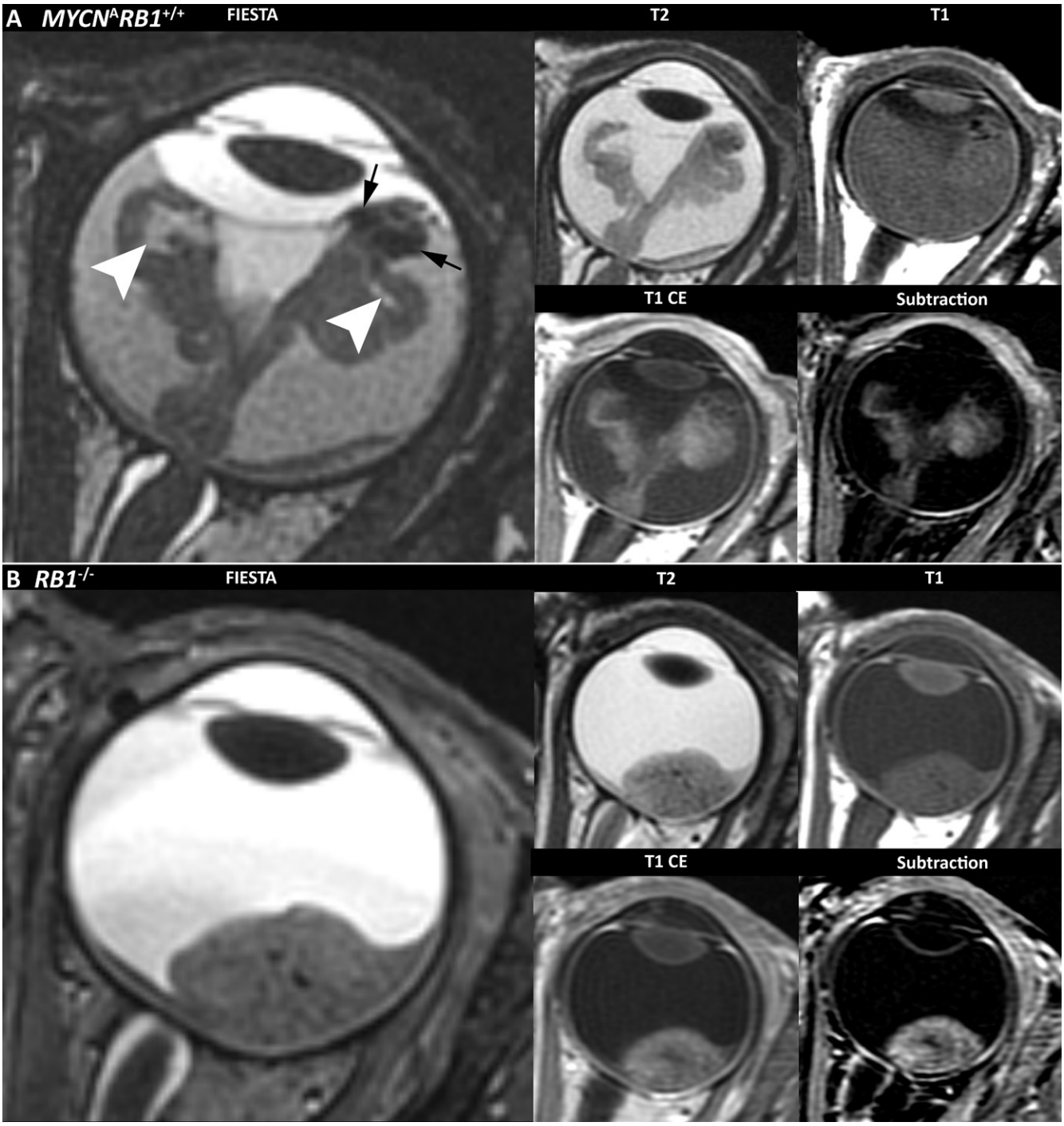

Figure 2: MRI phenotype *MYCN*-amplified *RB1* wild-type (*MYCN*^{A}*RB1*$^{+/+}$) retinoblastoma versus retinoblastoma driven by *RB1* pathogenic variation (*RB1*$^{-/-}$). **(A)** Representative MRI scans in a 42-month-old boy with *MYCN*^{A}*RB1*$^{+/+}$ retinoblastoma show relatively anterior tumor location, irregular margins, a pleomorphic shape, tumor-retinal folding with retina-retina contact (arrowheads), and peritumoral blood (arrows). Axial T1-weighted images with and without gadolinium-based contrast agent, T2-weighted image, and subtraction image are included. **(B)** MRI scan in a 10-month-old girl with *RB1*$^{-/-}$ retinoblastoma shows a posterior location, smooth margins, and a lens shape without vitreous inclusion or peritumoral blood. Axial T1-weighted images with and without gadolinium-based contrast agent, T2-weighted image, and subtraction image are included. CE = contrast enhanced, FIESTA = fast imaging employing steady-state acquisition.

(*MYCN*^{A}*RB1*$^{+/+}$, in 13 of 21 children [62%]; *RB1*$^{-/-}$, in 17 of 84 children [20%]; $P = .008$) (Fig 3).

Discussion

Because retinoblastomas driven by *MYCN* amplification (ie, *MYCN*^{A}*RB1*$^{+/+}$) have an aggressive nature and relative resistance to typical chemotherapy approaches, identification of patients with this retinoblastoma subtype is clinically important. As tissue biopsy is not safe in retinoblastoma, we sought to determine whether MRI could be used to identify this rare retinoblastoma subtype. Compared with retinoblastoma driven by biallelic pathogenic variation of *RB1* (ie, *RB1*$^{-/-}$), *MYCN*^{A}*RB1*$^{+/+}$ tumors

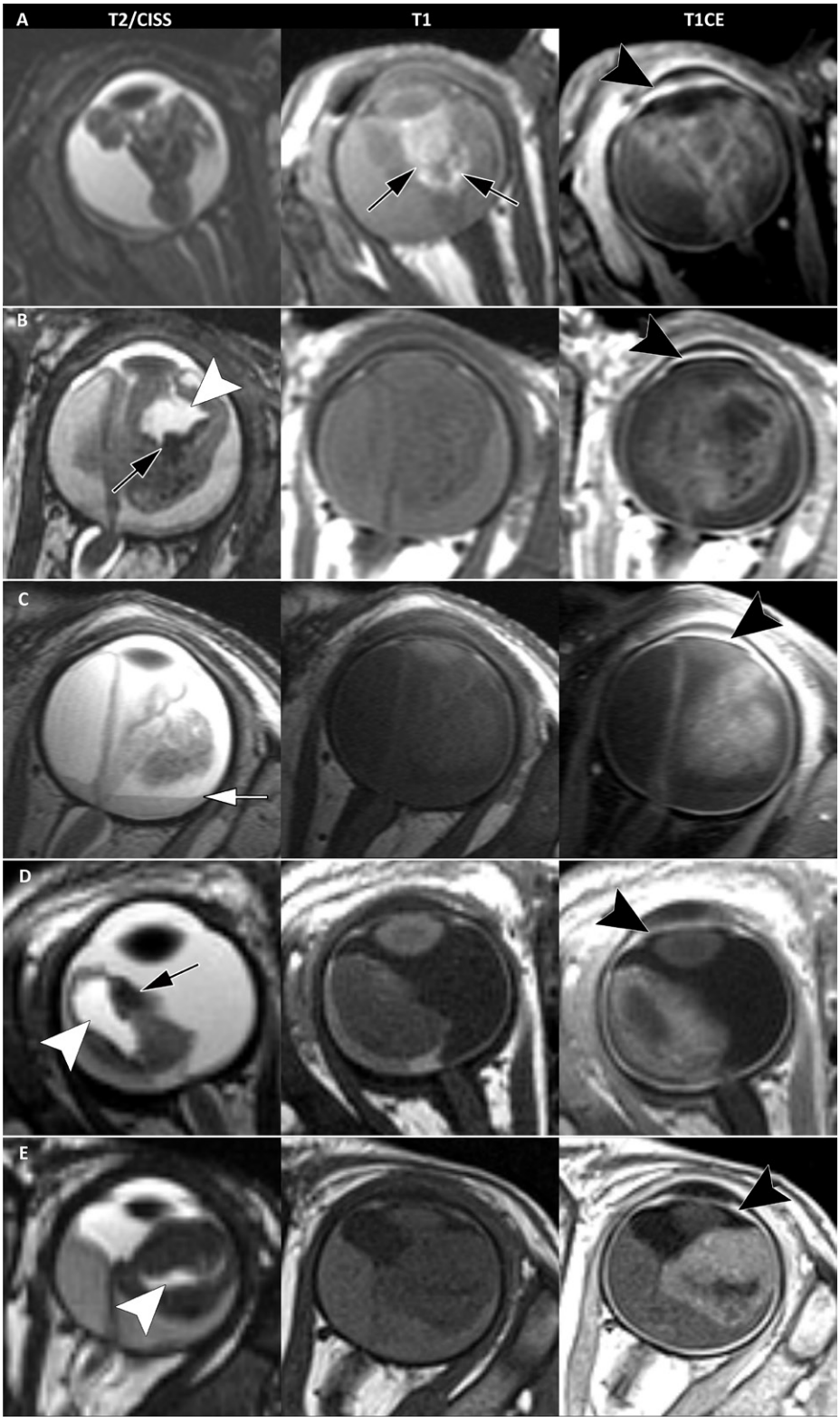

Figure 3: Example T2-weighted constructive interference in steady state (CISS), T1-weighted noncontrast, and T1-weighted contrast-enhanced (CE) images in five children with *MYCN*-amplified *RB1* wild-type ($MYCN^{A}RB1^{+/+}$) retinoblastoma show typical MRI phenotypes in an **(A)** 11-month-old boy, **(B)** 4-month-old girl, **(C)** 6-month-old boy, **(D)** 3-month-old girl, and **(E)** 4-month-old girl. Typical MRI features include anterior tumor location, irregular tumor margins, plaque or pleomorphic shape, a diffuse growth pattern, and numerous tumor lesions. Peritumoral hemorrhage is shown (black arrows in **A**, **B**, and **D**). T1 hyperintensity suggests the presence of peritumoral blood in **A**. Subretinal hemorrhagic fluid-fluid level is shown (white arrow in **C**). Tumor-retina folding with enclosure of the vitreous is denoted (white arrowheads in **B**, **D**, and **E**). Strong enhancement of the anterior eye segment is present in all five patients (black arrowheads on T1-weighted sequences with gadolinium-based contrast agent).

were recognizable at pretreatment MRI by their peripheral location anteriorly to the equator (specificity, 97%; $P < .001$), irregular margins (specificity, 70%; $P = .008$), diffuse growth pattern ($P = .044$) with many tumor foci ($P = .005$), peritumoral hemorrhage (specificity, 88%; $P < .001$), and extensive folding of the affected retina enclosing parts of the vitreous (specificity, 94%; $P < .001$). These imaging findings could supplement clinical findings, such as unilaterality and young age, for pretreatment recognition of $MYCN^{A}RB1^{+/+}$ retinoblastoma.

The diffuse growth pattern, irregular margins, and multiple tumor foci found at MRI in $MYCN^{A}RB1^{+/+}$ retinoblastoma may suggest rapid tumor growth at a young age. Aggressive tumor growth and young age were also described in clinical evaluations (2). Children with $MYCN^{A}RB1^{+/+}$ retinoblastoma in our study had a median age of 7 months, considerably younger than patient population with unilateral $RB1^{-/-}$ retinoblastoma (approximately 24 months [17]). The finding of a peripheral location anteriorly to the equator at MRI was surprising in these young children, considering retinal development proceeds from center (posterior) to periphery (anterior). Most of the retina was affected in these patients, suggesting either fast tumor growth from posterior to anterior or extensive multifocality. A peripheral location by itself is, unlike the other described features for $MYCN^{A}RB1^{+/+}$ tumors, not a sign of advanced-stage disease in the population with general ($RB1^{-/-}$) retinoblastoma. The peripheral location may, however, lead to a diagnosis at a relatively advanced stage in the absence of leukocoria as an early symptom, as seen in central tumors. In children with $RB1^{-/-}$ retinoblastoma, tumors originating from the peripheral retina are seen in patients of older age, mostly with an unaffected central (posterior) retina (18). Fast tumor growth is also a possible explanation for other imaging features of $MYCN^{A}RB1^{+/+}$ tumors.

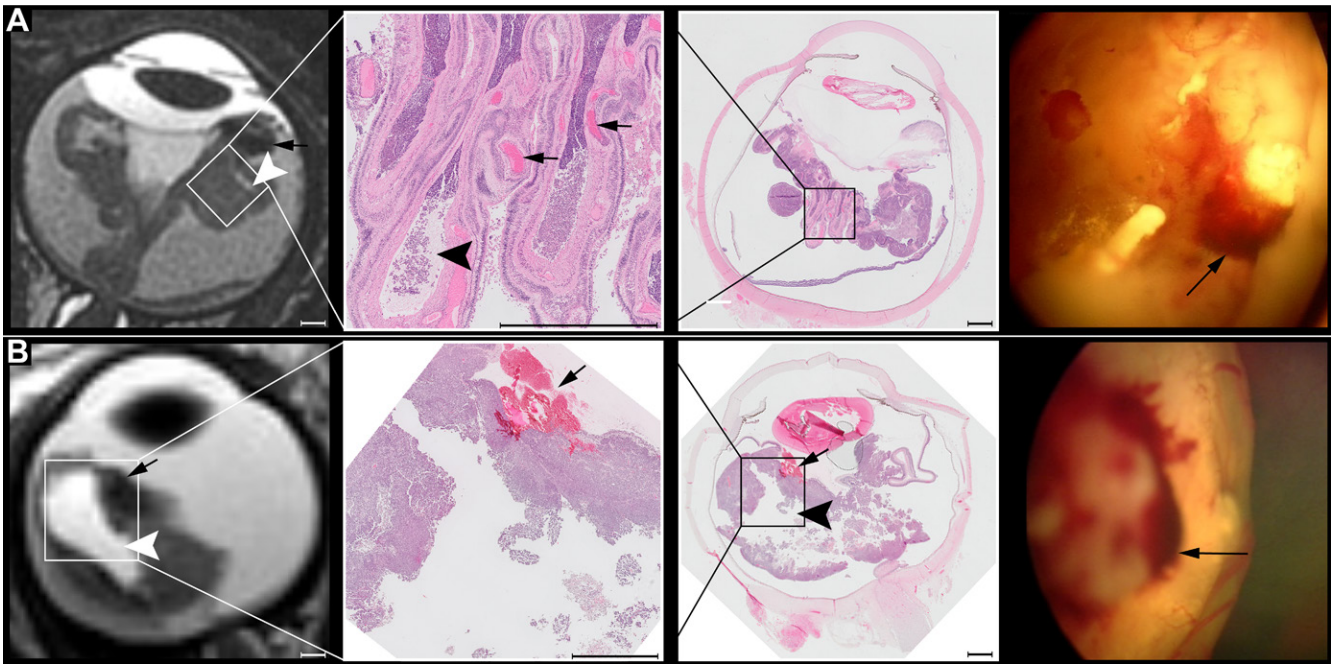

Figure 4: Axial MRI scans (left column), histopathologic images (middle columns), and fundoscopic images (right column) in two children with *MYCN*-amplified *RB1* wild-type (ie, *MYCN*^{A}*RB1*$^{+/+}$) retinoblastoma, **(A)** a 42-month-old boy and **(B)** 3-month-old girl. MRI scans show peritumoral hemorrhage (black arrows) and retinal detachment with multiple retinal folds with vitreous enclosure (black and white arrowheads). Scale bars of 25 mm are shown in the bottom right corner. Fundoscopic images show extensive peritumoral blood (black arrows, without spatial correlation).

For instance, the folding of a tumor-filled retina with vitreous enclosure is probably caused by rapid growth in a convoluting manner, in which one fold of the retina attaches to an opposite fold. In our study, this was confirmed at histopathologic evaluation. These vitreous invaginations were large and often unifocal compared with multifocal smaller cavitations seen in cavitary retinoblastoma (19). Peritumoral hemorrhage and subretinal hemorrhage with fluid-fluid levels could also be related to fast tumor growth. These MRI features are likely due to the tumor outgrowing its blood supply, resulting in hypoxia. Hypoxia induces upregulation of proangiogenic factors, including the vascular endothelial growth factor gene, resulting in the formation of fragile blood vessels that may hemorrhage more easily (20). This may also explain the frequent finding of anterior eye segment enhancement in *MYCN*^{A}*RB1*$^{+/+}$ retinoblastoma: poorly developed regions of the blood-ocular barrier possibly result in extravascular leakage of contrast material into the anterior eye chamber (21). We suggest that the majority of imaging findings in patients with *MYCN*^{A}*RB1*$^{+/+}$ retinoblastoma reflect the early onset and fast growth of this subtype, which is congruent with clinical, histopathologic, and molecular findings from previously described patients with this retinoblastoma subtype (2,8,22–24).

In addition to supporting the previously established difference in molecular makeup and histopathologic appearance, our study also showed that *MYCN*^{A}*RB1*$^{+/+}$ tumors have a unique phenotypic appearance at MRI (2–4,8). This provides further evidence that *MYCN*^{A}*RB1*$^{+/+}$ is a distinct retinoblastoma subtype with different behavior from *RB1*$^{-/-}$, potentially benefiting from new targeted treatments. In a recent study, a novel therapy (MLN4924 [Pevonedistat, Takeda], a neddylation inhibitor) was tested in human retinoblastoma xenografts in vivo, and chemosensitivity was observed in both *MYCN*^{A}*RB1*$^{+/+}$ and *RB1*$^{-/-}$ tumors (25). Such compounds may be specifically valuable in treatment of *MYCN*^{A}*RB1*$^{+/+}$ retinoblastoma, as these tumors have been described to respond poorly to traditional chemotherapeutic regimens (8). Another described approach includes the use of anti-GD2 monoclonal antibodies, since chemorefractory *MYCN*^{A}*RB1*$^{+/+}$ retinoblastoma has been shown to express ganglioside GD2 (26). Multiple compounds for *MYC* inhibition have entered clinical-phase research, although more research is needed to bring therapies from bench to bedside (27). In both research and clinical settings, MRI features can aid in patient selection for targeted treatments against the *MYCN*^{A}*RB1*$^{+/+}$ subtype (26).

Our study had several limitations. First, the subtype *MYCN*^{A}*RB1*$^{+/+}$ is rare, and available MRI data are limited. We had to acquire data internationally from multiple centers, and MRI protocols and quality varied. Generally, MRI requirements for retinoblastoma include a field strength above 1.5 T, a section thickness of less than 2 mm, a T2-weighted sequence, and T1-weighted sequences before and after intravenous administration of a gadolinium-based contrast agent (13). Second, interreader agreement of imaging features showed a wide range, possibly explained in part by insufficient MRI quality for features requiring detailed evaluation. Third, the low prevalence of the *MYCN*^{A}*RB1*$^{+/+}$ subtype resulted in large CIs for prediction parameters for morphologic features.

In conclusion, *MYCN*-amplified *RB1* wild-type retinoblastomas show distinct MRI features that could enable early identification of this more aggressive retinoblastoma subtype.

Author contributions: Guarantors of integrity of entire study, **R.W.J., C.M.d.B., P.M., P.d.G.**; study concepts/study design or data acquisition or data analysis/interpretation, all authors; manuscript drafting or manuscript revision for important intellectual content, all authors; approval of final version of submitted manuscript, all authors; agrees to ensure any questions related to the work are appropriately resolved, all authors; literature research, **R.W.J., C.M.d.B., A.H.S., P.M., S. Sirin, J.A.C., P.v.d.V., J.D.**; clinical studies, **C.M.d.B., J.L.J., A.H.S., A.K.M., P.M., O.E.U., H.G., R.C.B., S. Sen, S. Sirin, H.J.B., P.G., C.J.D., J.A.C., P.v.d.V., A.C.M., P.d.G.**; experimental studies, **R.W.J., S.v.E., S. Sen, J.A.C., P.v.d.V., R.B., J.D.**; statistical analysis, **R.W.J., C.M.d.B., M.C.d.J.**; and manuscript editing, **R.W.J., C.M.d.B., L.C., S.G., S.v.E., J.L.J., A.R., A.H.S., A.K.M., P.M., O.E.U., G.B.H., H.C.B., K.E.N., R.C.B., S. Sen, S. Sirin, H.J.B., C.J.D., J.A.C., P.v.d.V., R.B., J.D., A.C.M., M.C.d.J., P.d.G.**

Data sharing: Data generated or analyzed during the study are available from the corresponding author by request.

Disclosures of conflicts of interest: **R.W.J.** No relevant relationships. **C.M.d.B.** No relevant relationships. **L.C.** No relevant relationships. **S.G.** No relevant relationships. **S.v.E.** No relevant relationships. **J.L.J.** No relevant relationships. **A.R.** No relevant relationships. **A.H.S.** Consulting fees from Castle Biosciences; payment for lecture at Immunocore educational symposium; support for travel from Immunocore. **A.K.M.** No relevant relationships. **P.M.** No relevant relationships. **O.E.U.** No relevant relationships. **G.B.H.** No relevant relationships. **H.G.** No relevant relationships. **H.C.B.** No relevant relationships. **K.E.N.** No relevant relationships. **R.C.B.** Consultant for Aileron Therapeutics. **S. Sen** No relevant relationships. **S. Sirin** No relevant relationships. **H.J.B.** No relevant relationships. **P.G.** No relevant relationships. **C.J.D.** No relevant relationships. **J.A.C.** No relevant relationships. **P.v.d.V.** No relevant relationships. **R.B.** No relevant relationships. **J.D.** No relevant relationships. **A.C.M.** No relevant relationships. **M.C.d.J.** No relevant relationships. **P.d.G.** No relevant relationships.

References

1. Moll AC, Kuik DJ, Bouter LM, et al. Incidence and survival of retinoblastoma in the Netherlands: a register based study 1862-1995. Br J Ophthalmol 1997;81(7):559–562.
2. Rushlow DE, Mol BM, Kennett JY, et al. Characterisation of retinoblastomas without RB1 mutations: genomic, gene expression, and clinical studies. Lancet Oncol 2013;14(4):327–334.
3. Ewens KG, Bhatti TR, Moran KA, et al. Phosphorylation of pRb: mechanism for RB pathway inactivation in *MYCN*-amplified retinoblastoma. Cancer Med 2017;6(3):619–630.
4. Singh HP, Shayler DWH, Fernandez GE, et al. An immature, dedifferentiated, and lineage-deconstrained cone precursor origin of N-Myc-initiated retinoblastoma. Proc Natl Acad Sci U S A 2022;119(28):e2200721119.
5. Blixt MKE, Hellsand M, Konjusha D, et al. *MYCN* induces cell-specific tumorigenic growth in *RB1*-proficient human retinal organoid and chicken retina models of retinoblastoma. Oncogenesis 2022;11(1):34.
6. Price EA, Patel R, Scheimberg I, et al. *MYCN* amplification levels in primary retinoblastoma tumors analyzed by Multiple Ligation-dependent Probe Amplification. Ophthalmic Genet 2021;42(5):604–611.
7. Lillington DM, Goff LK, Kingston JE, et al. High level amplification of N-MYC is not associated with adverse histology or outcome in primary retinoblastoma tumours. Br J Cancer 2002;87(7):779–782.
8. Zugbi S, Ganiewich D, Bhattacharyya A, et al. Clinical, genomic, and pharmacological study of *MYCN*-amplified *RB1* wild-type metastatic retinoblastoma. Cancers (Basel) 2020;12(9):2714.
9. Abramson DH, Gobin YP, Francis JH. Orbital retinoblastoma treated with intra-arterial chemotherapy. Ophthalmology 2021;128(10):1437.
10. Zhou C, Wen X, Ding Y, et al. Eye-preserving therapies for advanced retinoblastoma: a multicenter cohort of 1678 patients in China. Ophthalmology 2022;129(2):209–219.
11. Berry JL, Xu L, Kooi I, et al. Genomic cfDNA analysis of aqueous humor in retinoblastoma predicts eye salvage: the surrogate tumor biopsy for retinoblastoma. Mol Cancer Res 2018;16(11):1701–1712.
12. De Jong MC, van der Meer FJ, Göricke SL, et al. Diagnostic accuracy of intraocular tumor size measured with MR imaging in the prediction of postlaminar optic nerve invasion and massive choroidal invasion of retinoblastoma. Radiology 2016;279(3):817–826.
13. de Graaf P, Göricke S, Rodjan F, et al. Guidelines for imaging retinoblastoma: imaging principles and MRI standardization. Pediatr Radiol 2012;42(1):2–14.
14. de Jong MC, Kors WA, de Graaf P, Castelijns JA, Kivelä T, Moll AC. Trilateral retinoblastoma: a systematic review and meta-analysis. Lancet Oncol 2014;15(10):1157–1167.
15. Jansen RW, de Bloeme CM, Brisse HJ, et al. MR imaging features to differentiate retinoblastoma from Coats' disease and persistent fetal vasculature. Cancers (Basel) 2020;12(12):3592.
16. Jansen RW, de Jong MC, Kooi IE, et al. MR imaging features of retinoblastoma: association with gene expression profiles. Radiology 2018;288(2):506–515.
17. Broaddus E, Topham A, Singh AD. Incidence of retinoblastoma in the USA: 1975-2004. Br J Ophthalmol 2009;93(1):21–23.
18. King BA, Parra C, Li Y, et al. Spatiotemporal patterns of tumor occurrence in children with intraocular retinoblastoma. PLoS One 2015;10(7):e0132932.
19. Raval V, Kaliki S. Cavitary retinoblastoma: a review of literature. Surv Ophthalmol 2022;67(3):723–728.
20. Stitt AW, Simpson DA, Boocock C, Gardiner TA, Murphy GM, Archer DB. Expression of vascular endothelial growth factor (VEGF) and its receptors is regulated in eyes with intra-ocular tumours. J Pathol 1998;186(3):306–312.
21. de Graaf P, van der Valk P, Moll AC, et al. Contrast-enhancement of the anterior eye segment in patients with retinoblastoma: correlation between clinical, MR imaging, and histopathologic findings. AJNR Am J Neuroradiol 2010;31(2):237–245.
22. Moulin AP, Stathopoulos C, Marcelli F, Schoumans Pouw J, Beck-Popovic M, Munier FL. Secondary enucleated retinoblastoma with MYCN amplification. Ophthalmic Genet 2021;42(3):354–359.
23. Afshar AR, Pekmezci M, Bloomer MM, et al. Next-generation sequencing of retinoblastoma identifies pathogenic alterations beyond *RB1* inactivation that correlate with aggressive histopathologic features. Ophthalmology 2020;127(6):804–813.
24. Roohollahi K, de Jong Y, van Mil SE, Fabius AWM, Moll AC, Dorsman JC. High-level *MYCN*-amplified *RB1*-proficient retinoblastoma tumors retain distinct molecular signatures. Ophthalmol Sci 2022;2(3):100188.
25. Aubry A, Yu T, Bremner R. Preclinical studies reveal MLN4924 is a promising new retinoblastoma therapy. Cell Death Discov 2020;6(1):2.
26. Schaiquevich P, Francis JH, Cancela MB, Carcaboso AM, Chantada GL, Abramson DH. Treatment of retinoblastoma: what is the latest and what is the future. Front Oncol 2022;12:822330.
27. Llombart V, Mansour MR. Therapeutic targeting of "undruggable" MYC. EBioMedicine 2022;75:103756.